Russian Geology and Geophysics © 2020, V.S. Sobolev IGM, Siberian Branch of the RAS
Vol. 61, No. 2, pp. 155–173, 2019 *DOI:10.15372/RGG2019111* *Geologiya i Geofizika*

Mineralogical and Geochemical Features and Formation Conditions of the Tardan Gold–Sulfide–Quartz Deposit (Northeastern Tuva)

R.V. Kuzhuget[a, ✉], N.N. Ankusheva[b,c], I.R. Prokop'ev[d,e], A.A. Redina[d]

[a] *Tuva Institute for Exploration of Natural Resources, Siberian Branch of the Russian Academy of Sciences, ul. Internatsional'naya 117a, Kyzyl, 667007, Russia*

[b] *Institute of Mineralogy, South Urals Federal Research Center of Mineralogy and Geoecology, Ural Branch of the Russian Academy of Sciences, Il'menskii Zapovednik 1, Miass, 456317, Russia*

[c] *South Ural State University Branch, ul. 8 Iyulya 10, Miass, 456316, Russia*

[d] *V.S. Sobolev Institute of Geology and Mineralogy, Siberian Branch of the Russian Academy of Sciences, pr. Akademika Koptyuga 3, Novosibirsk, 630090, Russia*

[e] *Novosibirsk State University, ul. Pirogova 1, Novosibirsk, 630090, Russia*

Received 15 August 2018; received in revised form 25 December 2018; accepted 21 March 2019

Abstract—We studied the mineralogical and geochemical features and formation conditions of productive mineral assemblages of the Tardan gold–sulfide–quartz deposit located in the endo-/exocontact zone of the Kopto–Bai-Syut gabbro-diorite–plagiogranite pluton of the Early Ordovician Tannu-Ola complex (O_1tn). Postskarn mineralization of vein–dissemination type in skarns, quartz diorites, and carbonate rocks is limited by tectonic crushing zones and conjugated with beresitization and listwanitization of the ore-bearing rocks. Mineralogical and geochemical research has shown the formation of ultrahigh-fineness (986–952‰) and high-fineness (947–918‰) gold at the first productive gold–quartz–calcite substage, of high-fineness gold (918–904‰) → medium-fineness gold (896–809‰) → low-fineness gold (798–756‰) ± hessite Ag_2Te ± volynskite $AgBiTe_2$ at the second productive gold–telluride–sulfide–quartz–carbonate substage, and of medium-fineness gold (897–802‰) → low-fineness gold (799–717‰) → electrum (691–612‰) → mercurian electrum (471–451‰) ± hessite Ag_2Te ± acanthite Ag_2S ± matildite $AgBiS_2$ at the third productive gold–sulfosalt–sulfide–quartz substage. High- and medium-fineness gold prevails in the ores, ultrahigh- and low-fineness gold is subordinate, and electrum and mercurian electrum are scarce. The fineness of native gold in the ores varies from 451 to 986‰, averaging 858‰. The productive mineral assemblages of the Tardan deposit formed from aqueous fluids containing Mg, Na, and K chlorides (salinity of 6.1–12.9 wt.% NaCl eq.), with a decrease in the mineral formation temperature from 380 to 150 ºC and variations in f_{O2}, f_{S2}, f_{Se2}, and f_{Te2}.

Keywords: native gold, hydrothermal gold deposits, fluid inclusions, Tuva

INTRODUCTION

In recent years, investigations at the Murzinskoe, Sinyukhinskoe, Tardan (Russia), Zarkashan (Afghanistan), Khantauskoe, and Baksinskoe (Kazakhstan) deposits of the gold-skarn formation have shown that their gold-bearing mineral assemblages formed later than skarns and are associated with medium-temperature metasomatites of beresite–listwanite association. These metasomatites are developed after magnesian and calcareous skarns, volcanics, granitoids, and schists in brecciated and tectonic zones (Korobeinikov and Zotov, 2006; Gas'kov, 2008; Rafailovich and Shevchuk, 2010; Rafailovich, 2013). Calcareous and magnesian skarns contain significant amounts of Au only in zones where they are listwanitized (Spiridonov, 2010). The research has also revealed a spatial association of several ore formation types in gold ore objects, including porphyry gold–copper, gold-quartz (gold–sulfide–quartz) beresite–listwanite, and epithermal gold–silver (Rafailovich and Shevchuk, 2010; Rafailovich, 2013).

Gold ore objects in skarns are widespread in the geologic structures of Tuva, but their commercial assessment is difficult because of the limited information about the mineralogical, geochemical, and petrographic features of ores. The genesis of these objects is also debatable. Their orebodies usually have high contents of well-recoverable gold but are of very intricate morphology and small size.

In the area of the Tardan ore cluster, prospecting works performed in 1963–1971 revealed gold ore objects in skarns (Tardan, Soruglug-Khem, Barsuchii, Kopto, and Pravoberezhnoe deposits) and beresites (Tardan-2 ore occurrence), as well as a number of small gold ore occurrences and mineral-

✉ Corresponding author.
E-mail address: rkuzhuget@mail.ru (R.V. Kuzhuget)

ization spots. Earlier, the deposits of this ore cluster in skarns were attributed to a commercial gold skarn formation (Kil'chichakov et al., 1966). At present, new data on gold genesis in the Tardan ore cluster have been obtained. In the gold deposits of this ore cluster, the hydrothermal gold mineralization process is superposed on contact-metasomatic rocks and separated from skarns by a deformation gap expressed as crushing of the early objects of the skarn formation and their cementation and replacement by hydrothermal paragenesis (Gas'kov, 2008). Magmatism and ore-bearing magnesian and calcareous skarns, aposcarn metasomatites, and magnetite ores of the Tardan deposit have been studied in detail in contrast to superposed hydrothermal gold mineralization in skarns and postskarn metasomatites.

The aim of our research was to determine the mineralogical and geochemical features and formation conditions of the productive mineral assemblages of the Tardan deposit, the largest reference object of the Tardan ore cluster.

METHODS

Ore lump and crushed ore samples were taken from the deposit bedrocks in mines. Thorough mineralogical studies of ores included examination of onthogenetic characteristics (composition, structure, mineral zoning, and induction surfaces), the intersection of early mineral aggregates by late ones, the presence of fragments of early minerals in late mineral aggregates, etc. All this information served as criteria for elucidation of the sequence of mineral formation in the ores. The chemical composition of minerals was determined at the V.S. Sobolev Institute of Geology and Mineralogy SB RAS (IGM SB RAS), Novosibirsk, using a MIRA 3 LMU scanning electron microscope (Tescan Orsay Holding) with INCA Energy 450 + XMax 80 and INCA Wave 500 (Oxford Instruments Nanoanalysis Ltd) microanalysis systems. Gold and minerals (cubic solid solutions) of the system Au–Ag are described using the earlier accepted terminology (Vernadsky, 1914; Petrovskaya, 1973; Spiridonov, 2010): native gold (1000–700‰: ultrahigh-fineness (1000–950‰), high-fineness (950–900‰), medium-fineness (900–800‰), and low-fineness (800–700‰)), electrum (700–300‰), kustelite (300–100‰), and Au-bearing silver of fineness of <100‰. The physicochemical conditions of deposition of mineral assemblages were studied by thermometry, with geothermometers and geofugometers, and by examining parageneses.

Fluid inclusions were studied by microthermometry in the Laboratory of Thermobarogeochemistry of the Department of Geology of South Ural State University, Miass, and at the Analytical Center of IGM SB RAS, Novosibirsk. Thermometric measurements were performed using a TMS-600 Linkam heating stage with LinkSystem 32 DV-NC software and an Olympus BX51 microscope. The eutectic temperatures of fluid inclusions were interpreted using the data obtained by Borisenko (1977, 1982). The fluid salinity was determined from the melting point of ice (Bodnar and Vityk, 1994). The measurement results were processed with the Statistica 6.1 software. To evaluate the temperature of formation of mineral assemblages, we used the pyrite–pyrrhotite geothermometer, which also permits estimation of sulfur volatility. With this geothermometer, the temperature and sulfur volatility are determined from the points of intersection of the pyrrhotite composition isopleths with the pyrite–pyrrhotite solvus in the $\lg f_{S_2}$–$1/T$ K diagrams (Toulmin and Barton, 1964). The stability fields of major ore minerals of the Tardan deposit in the f_{S_2}–f_{Te_2} diagram were determined using data from Barton and Skinner (1979) and Afifi et al. (1988a,b).

GEODYNAMIC SETTING OF THE TARDAN DEPOSIT

Tuva is part of the Central Asian Orogenic Belt, an accretion–collision structure formed during the geodynamic evolution and closure of the Paleoasian Ocean (Zonenshain et al., 1990; Berzin et al., 1994; Yarmolyuk et al., 2003). The evolution of the regional geologic and tectonic structures was a prolonged multistage process with a successive change in geodynamic regimes (island-arc, 562–518 Ma; accretion–collision, 510–450 Ma; etc.) (Rudnev et al., 2015) corresponding to the stages of the geodynamic evolution of the Altai–Sayan folded area (ASFA). Tuva is part of this area, with its specific features (Distanov and Obolenskii, 1994).

The Tardan gold ore cluster is localized in the zone of: (a) Vendian–early Cambrian island-arc complexes of the Ondum subzone of the Tannu-Ola–Khamsara island-arc zone; (b) middle Cambrian–Ordovician collisional intrusive, mainly granitoid complexes; and (c) Silurian sediments of a residual trough (Berzin and Kungurtsev, 1996; Mongush, 2016).

The Early Ordovician age of gold mineralization of the Tardan deposit (481 ± 6.1 Ma) and intrusive rocks (484–479 Ma) of the Early Tannu-Ola complex (O_1tn), parageneticaly associated with the gold mineralization (Gas'kov, 2008; Rudnev et al., 2015), suggests that the deposit formed after the completion of the active stage of Cambrian–Ordovician accretion–collision events in the region.

GEOLOGIC STRUCTURE OF THE TARDAN DEPOSIT

The Tardan ore cluster is located in the south of the ASFA, in the Kaa-Khem subzone of the East Tuva structure-facies zone and the Kaa-Khem deep fault in the margin of the Kaa-Khem polychronous batholith represented by the Kopto–Bai-Syut massif. Gold mineralization of the ore cluster is controlled by faults of the Kaa-Khem deep fault (Kudryavtseva, 1969; Korobeinikov et al., 1987; Korobeinikov and Zotov, 2006).

Gold ore objects are localized in the zone of contact of the Kopto–Bai-Syut gabbro-diorite–plagiogranite massif of the Early Ordovician Tannu-Ola complex (O_1tn) with volcanic carbonate rocks of the Tumat-Taiga (R–$Є_1$tt) and Tapsy ($Є_1$tp) Formations. The Ar/Ar biotite age of plagiogranites of the Kopto-Bai-Syut massif is 485.7 ± 4.4 Ma (Gas'kov, 2008), and the U–Pb zircon age is 479 ± 2 Ma (Rudnev et al., 2015).

The Tardan deposit was discovered during the prospecting for gold in 1964. It is localized in the zone of the exo-/endocontact of the Kopto–Bai-Syut massif (O_1tn) with late Riphean–early Cambrian volcanosedimentary: rocks of the Tumat-Taiga Formation (R–$Є_1$tt) (quartz porphyry, diabase porphyrites, and tuffs with dolomite interbeds) and, upsection, the Tapsa Formation ($Є_1$tp) (carbonate rocks with interbeds of felsic effusive rocks) (Fig. 1). The contact has a complex configuration in plan and is accompanied by numerous apophyses. Mineralization is controlled by faults of NE and NW strikes. The major Changys, Vostochnyi (Eastern), and Bezymyannyi faults are feathered by numerous small shear and detachment faults (Vakhrushev, 1972; Korobeinikov and Matsyushevskii, 1976; Gas'kov, 2008; Sovluk, 2010).

At the early stage (magnetite skarn formation), the intrusion of the Early Tannu-Ola diorite–tonalite–plagiogranite complex (O_1tn) led to the formation of magnesian (spinel–pyroxene, spinel–pyroxene–pargasite–phlogopite, and spinel–pyroxene–gehlenite) and calcareous (wollastonite, pyroxene, and pyroxene–garnet) skarns at the contact of diorites with late Riphean–early Cambrian carbonate rocks. These skarns are described in detail elsewhere (Vakhrushev, 1972; Korobeinikov and Matsyushevskii, 1976; Korobeinikov and Zotov, 2006).

Magnesian skarns are cut and replaced by calcareous skarns and are found as relics of replacement by diopside–garnet assemblages. A decrease in the temperature of the skarn formation process led to the formation of magnetite ores. They are accompanied by aposcarn tremolite–actinolite–chlorite, magnetite–actinolite–tremolite, serpentine, and quartz–hematite metasomatites, which appear at the sites of crushed magnesian and calcareous skarns. These aposcarn metasomatites coexist, composing zones of skarns altered by hydrothermal solutions. Many skarns are almost totally replaced by aposkarn associations, which is expressed as zoning of aposcarn metasomatites. The central sites of the zones contain small magnetite lenses (10–70 m long and 1–4 m thick) with tremolite–actinolite and chlorite–serpentine–carbonate rims 10–15 m and more in thickness.

The hydrothermal gold ore formation process was accompanied by the intense tectonic crushing of skarns and aposkarn magnetite–tremolite metasomatites and the intrusion of aplite, granite porphyry, and quartz porphyry dikes of the Early Tannu-Ola complex (O_1tn), resulted from the postmagmatic hydrothermal ore formation process. That is, the Tardan gold mineralization is of postskarn genesis and is spatially associated with skarn formation. In the ore field of the deposit, the Ar/Ar biotite age of small granite porphyry bodies (stocks and dikes) of the Early Tannu-Ola complex (O_1tn), paragenetically associated with gold ore mineralization, is 484.2 ± 4.3 Ma, and the age of gold mineralization determined by Ar/Ar dating of sericite from quartz veinlets of mineralized crushing zones is 481 ± 6.1 Ma, i.e., Early Ordovician (Gas'kov, 2008).

The superposed hydrothermal gold mineralization in skarns and aposkarn metasomatites is localized in skarn crushing zones along the contacts of intrusive rocks with limestones and in limestone crushing zones. The wallrock alteration was expressed as listwanitization of skarns and, to a lesser extent, beresitization of granite porphyry (up to 20–40 cm). The latter are accompanied by sericite–quartz metasomatites with chlorite, carbonate, and pyrite. The aureoles of wallrock-altered skarns are several times larger than the gold ore columns.

At present, there are 16 known ore zones with 41 orebodies at the Tardan deposit. The ore zones are 100–300 m long and 10 to 50–80 m thick. Orebodies are traceable for 50–200 m and vary in thickness from few meters to 13 m. Almost all ore zones are confined to the contact of diorites of the Early Tannu-Ola complex (O_1tn) with limestones of the Tapsy Formation ($Є_1$tp). The ore zones and orebodies are of NE, NW, and, seldom, N–S and E–W strikes. Orebodies in skarns are listwanitization zones in magnesian and calcareous skarns with veinlet-disseminated and nest quartz–carbonate–gold–sulfide segregations. The shape of the orebodies is governed by the spatial localization of productive mineral assemblages in the host rocks and is controlled by the rock fracturing. The orebodies are usually conformal with respect to the host skarns. Gold is unevenly distributed; its higher contents are observed in quartz–veinlet stockworks cementing crushed skarns developed in limestones. The organic matter of the limestones and infiltration skarns among them served as a geochemical barrier for the deposition of gold, which is confirmed by geological data: The commercial contents of gold in ore columns are found at the sites (intervals) where the host rocks contain organic matter.

The content of sulfides in the ores varies from 1 to 7%, averaging 3%. Chalcopyrite, bornite, and pyrite are major sulfide minerals. The ores have Ag/Au = 0.10–50 (on average, <1 or, seldom, <10). The granulometric composition of gold varies insignificantly; the predominant fractions are 0.25–0.10 (80%), 0.50–0.25 mm (10%), and <0.1 mm (9%), and the subordinate ones are 1.0–0.5 mm (0.9%) and 3.0–1.0 mm (<0.1%) (Korobeinikov and Matsyushevskii, 1976).

PRODUCTIVE MINERAL ASSEMBLAGES

Taking into account the previous research works (Korobeinikov and Zotov, 2006; Gusev, 2014) and our observations, we have established that the Tardan deposit formed in six substages: (1) pre-ore listwanite–beresite, (2) productive gold–quartz–calcite, (3) gold–telluride–sulfide–quartz–

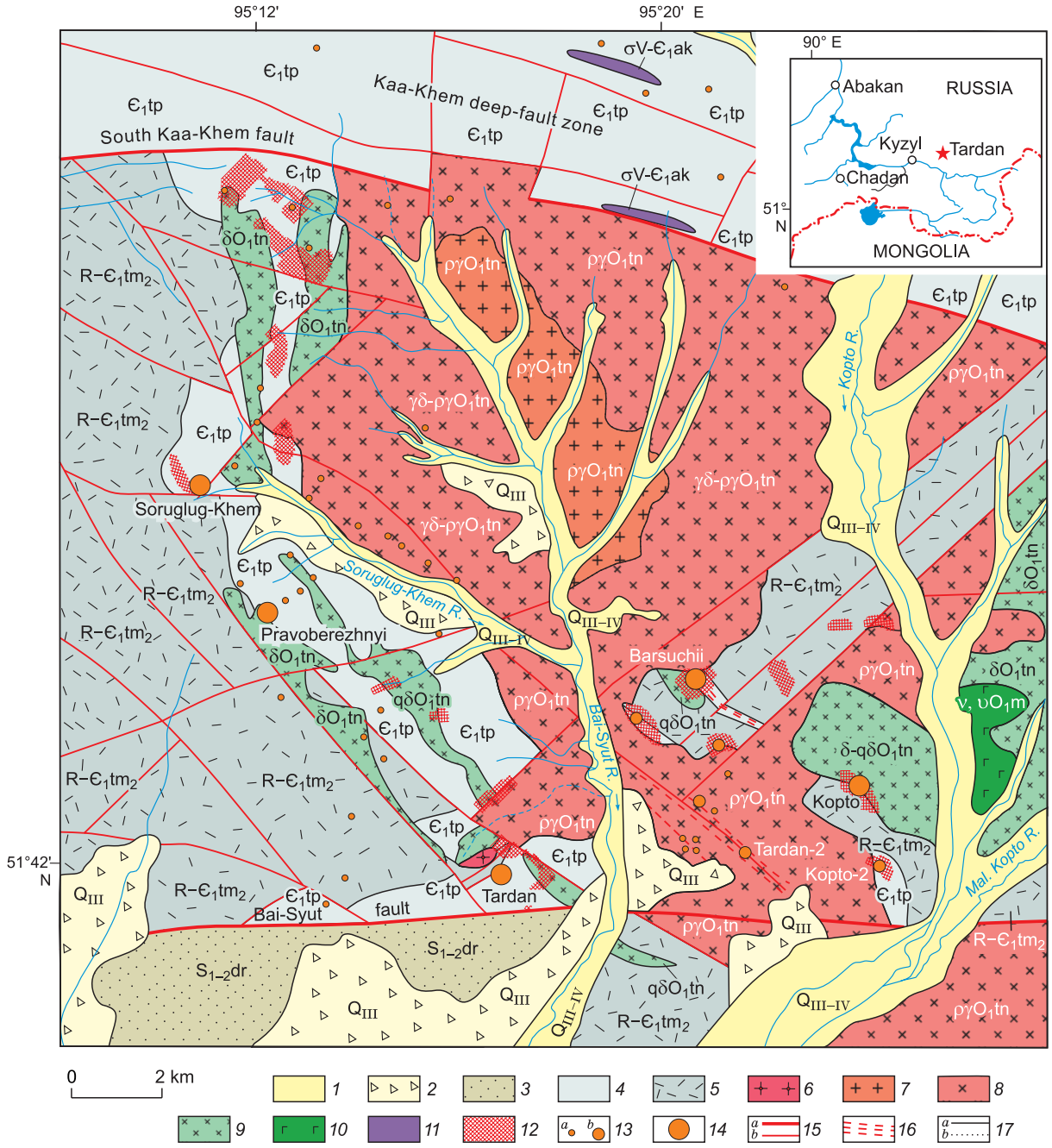

Fig. 1. Geological structure scheme of the Tardan gold ore cluster, after Kil'chichakov et al. (1966) and Rudnev et al. (2006, 2015), modified. *1,* alluvial floodplain sediments ($Q_{III–IV}$); *2,* deluvial–proluvial deposits (Q_{III}); *3,* red-colored sandstones, gravelstones, and conglomerates with interbeds of limestones of the Derzig Formation ($S_{1–2}$dr); *4,* sandstones, tuffstones, tuff gravelstones, siltstones, conglomerates, schists, amphibole–chlorite schists, and limestones of the Tapsy Formation ($Є_1$tp); *5,* basaltic and andesitic porphyrites with interbeds of limestones of the Upper Tumat-Taiga Subformation (R–$Є_1$tm$_2$); *6–9,* Early Tannu-Ola diorite–tonalite–plagiogranite complex (O_1tn): *6,* granite porphyry (γπ); *7,* plagiogranites (ργ); *8,* undivided plagiogranites (ργ) and tonalites (γδ); *9,* diorites (δ), quartz diorites (qδ); *10,* gabbroids of the Mazhalyk peridotite–pyroxenite–gabbronorite complex (ν,υO_1m); *11,* serpentinites, peridotites, pyroxenites, and associated gabbroids and diorites of the Akdovrak ophiolite complex (σV–$Є_1$ak); *12,* skarns; *13,* gold mineralization (*a*) and gold ore occurrence (*b*) sites; *14,* gold deposits; *15,* regional (*a*) and local (*b*) faults; *16,* crushing zones; 17, geologic boundaries: proved (*a*) and predicted (*b*).

carbonate, (4) gold–sulfosalt–sulfide–quartz, (5) post-ore quartz–carbonate, and (6) chlorite–hematite–quartz (Table 1).

Pre-ore medium-temperature metasomatites of the listwanite–beresite series with quartz, pyrite, sericite, fuchsite, and ankerite formed during listwanitization of skarns and aposcarn metasomatites in tectonic crushing zones. The listwanitization zones form linear lenticular bodies in magnesian–calcareous skarns and magnetite–actinolite–tremolite–

Table 1. Sequence of mineral formation in the Tardan deposit

Mineral	Hydrothermal gold–sulfide–quartz substage						Hypergenesis substage
	1	2	3	4	5	6	
Quartz							
Calcite							
Dolomite							
Siderite							
Ankerite							
Sericite							
Fuchsite							
Pyrite							
Chlorite							
Albite							
Pyrrhotite							
Arsenopyrite							
Chalcopyrite							
Bornite							
Galena							
Se-galena							
Sphalerite							
Wittichenite							
Volynskite							
Tellurobismuthite							
Tetradymite							
Se-tetradymite							
Gold							
Electrum							
Mercurian electrum							
Hessite							
Acanthite							
Tennantite							
Bismuthite							
Native Bi							
Tsumoite							
Pilsenite							
Matildite							
Cobaltite							
Siegenite							
Glaucodot							
Barite							
Hematite							
Covellite							
Chalcocite							
Digenite							
Geerite							
Malachite							
Azurite							
Chrysocolla							
Smithsonite							
Cerussite							
Tenorite							
Bismutite							
Bismite							
Goethite							
Cuprite							
Native copper							

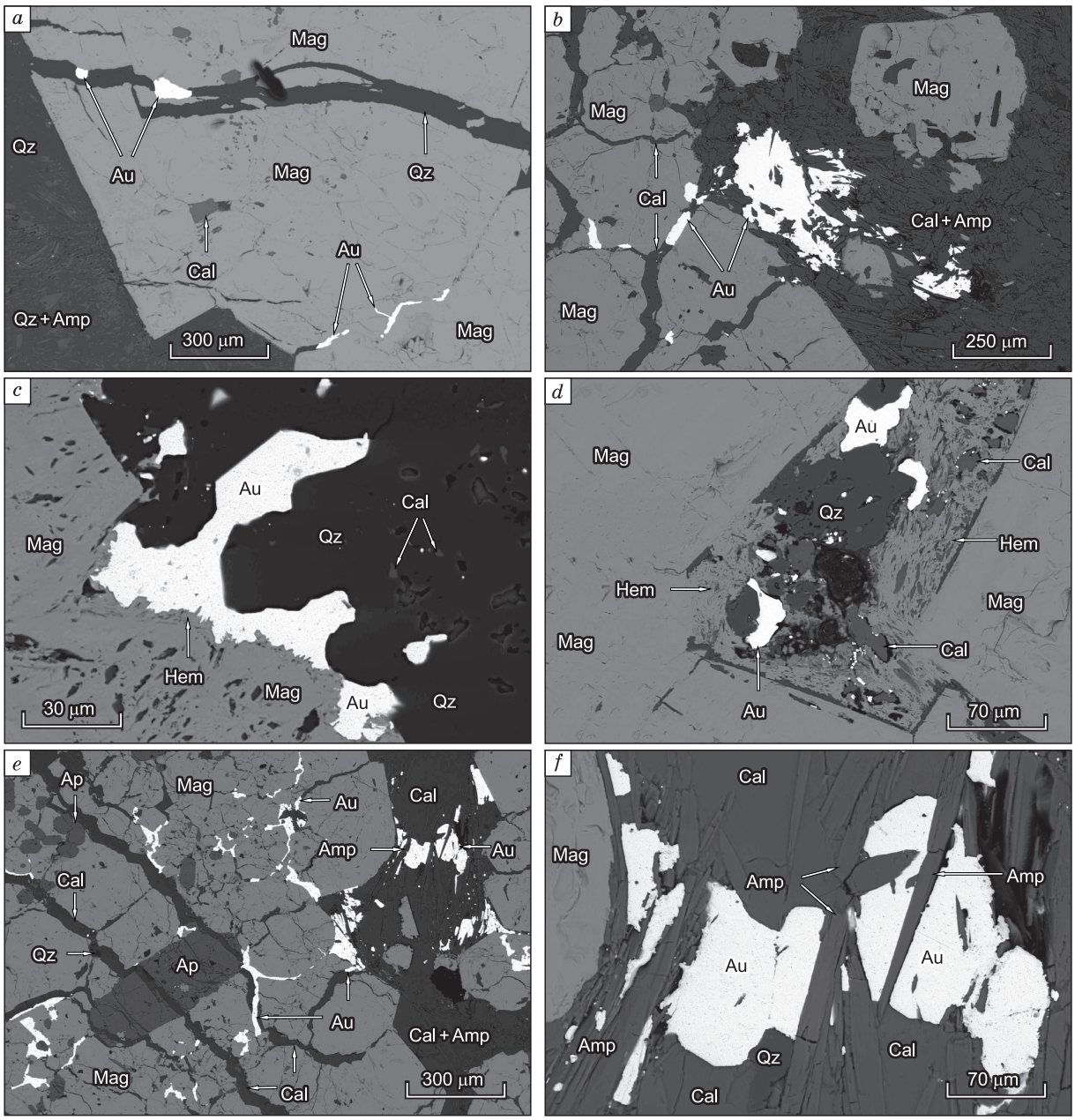

Fig. 2. Mineral assemblages of the early gold–quartz–calcite substage; gold (Au), quartz (Qz), and calcite (Cal) are localized at the sheared sites of magnetite–actinolite–tremolite metasomatites. Hem, hematite; Mag, magnetite; Ap, apatite; Amp, minerals of the tremolite–actinolite series. Hereafter, BSE images are presented.

chlorite metasomatites and bear veinlet-disseminated productive mineralization. Post-ore quartz–carbonate (calcite, ankerite, and quartz) and chlorite–hematite–quartz (quartz, chlorite, hematite, and albite) veinlets up to 4 mm thick cut mineral aggregates formed at the previous substages.

The oxidation zone of the deposit is widely pronounced, especially in fault and fracturing zones (to a depth of 50–100 m and greater). Chrysocolla, malachite, azurite, smithsonite, goethite, hydrogoethite, cerussite, covellite, chalcocite, digenite, cuprite, tenorite, geerite, bismutite, and native copper occur in the weathering crust.

Gold-bearing productive mineral assemblages have the following composition: (1) gold–quartz–calcite (quartz, calcite, gold ± pyrite ± pyrrhotite ± chalcopyrite ± arsenopyrite); (2) gold–telluride–sulfide–quartz–carbonate (calcite, quartz, chalcopyrite, bornite, pyrite, gold, wittichenite Cu_3BiS_3, volynskite $AgBiTe_2$, tellurobismuthite, tetradymite Bi_2Te_2S, Se-bearing tetradymite (up to 4.4 wt.% Se), galena, sphalerite (up to 0.5 wt.% Fe and up to 0.61 wt.% Cd) ± cobaltite); and (3) gold–sulfosalt–sulfide–quartz (quartz, calcite, chalcopyrite, pyrite, galena, Se-galena (up to 5 wt.% Se), sphalerite (up to 7.45 wt.% Fe), arsenopyrite,

gold, electrum, mercurian electrum ± hessite ± acanthite ± bismuthinite ± baryte ± native bismuth ± pilsenite Bi_4Te_3 ± matildite $AgBiS_2$ ± tsumoite BiTe ± siegenite $CoNi_2S_4$ ± glaucodot $CoFeAs_2S_2$).

Early gold–quartz–calcite mineralization with scarce pyrite, pyrrhotite, arsenopyrite, and chalcopyrite grains is found at the sheared sites of hematite–magnetite ores and magnetite–actinolite–tremolite metasomatites, in microcracks, and in the magnetite interstices. It is extremely unevenly distributed and occurs as fine clusters (up to 0.8 mm) and veins (up to 0.5 cm or, seldom, 2 cm) of gold–quartz–calcite composition (Fig. 2). Calcite is of two generations with compositions $Ca_{0.99}Mn_{0.01}CO_{3.00}$ and $Ca_{0.97–0.99}Fe_{0.01–0.02}Mn_{0.00–0.01}CO_{3.00}$.

Gold is found as golden-yellow fine thin (0.001–0.5 mm) segregations of interstitial, lumpy, and lump-branched shapes; crystals of octahedral and cuboctahedral habits are scarcer (Fig. 3). Native gold is of two types according to the content of silver:

(1) ultrahigh-fineness gold with Ag ≤ 5 wt.% (Au = 93.97–99.73; Ag = 0.93–4.80; Cu = 0.00–0.89; and Fe = 0.00–0.88 wt.%);

(2) high-fineness gold with Ag ≤ 8 wt.% (Au = 91.26–94.58; Ag = 5.08–7.87; Cu = 0.00–0.62; and Hg = 0.00–0.04 wt.%).

Gold–telluride–sulfide–quartz–carbonate mineralization of the second productive substage cuts the mineral aggregates of the first productive substage and is also superposed

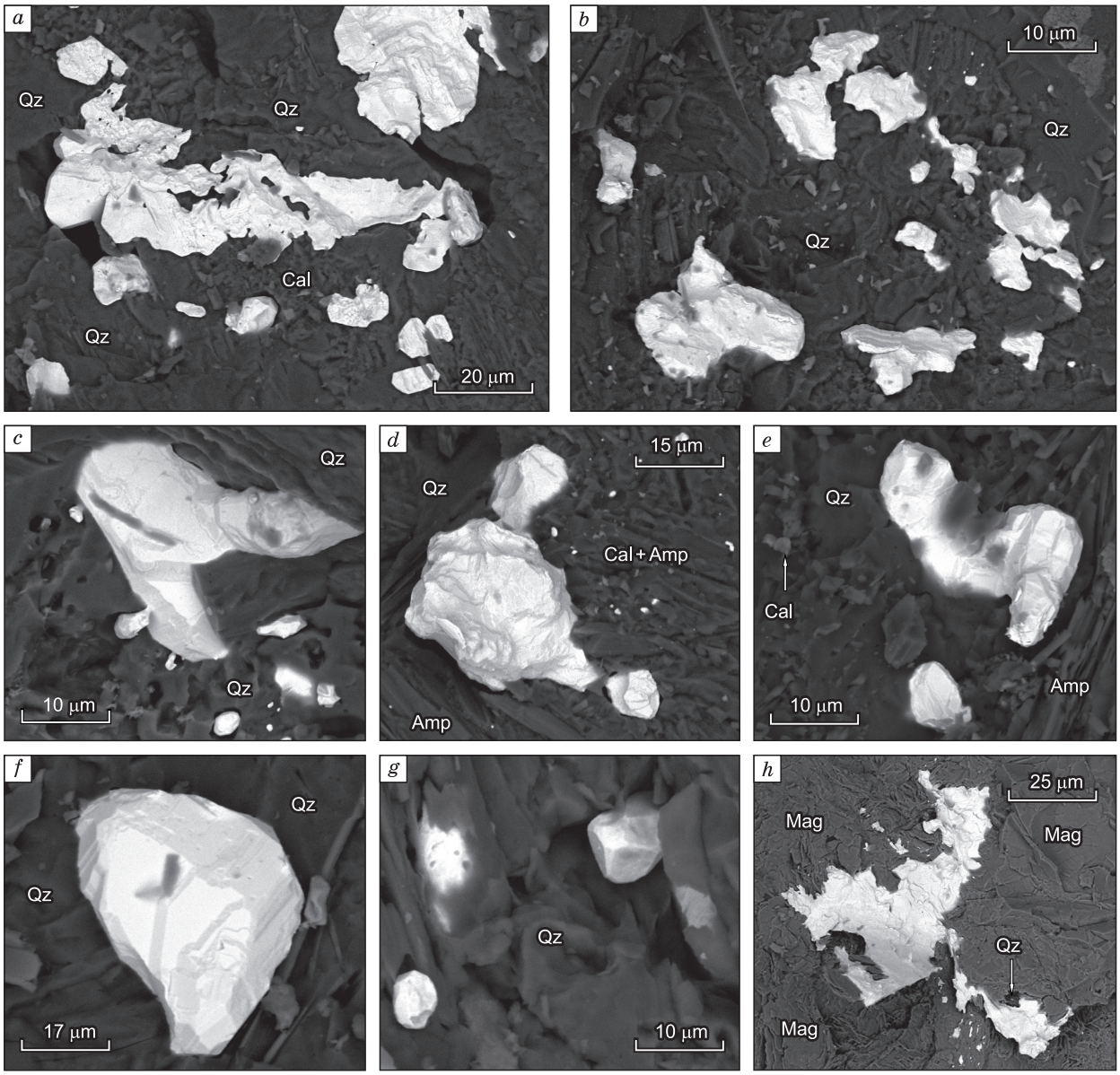

Fig. 3. Gold of the gold–quartz–calcite substage in quartz (Qz), calcite (Cal), magnetite (Mag), and minerals of the tremolite–actinolite series (Amp) of magnetite–actinolite–tremolite metasomatites.

on sheared skarns, hematite–magnetite ores, and volcanosedimentary, igneous, and listwanitized rocks in tectonic crushing zones. It is most widespread in the Tardan deposit and forms veinlet-disseminated and veinlet segregations of quartz and quartz–carbonate–sulfide composition and single thin (up to 50 cm) quartz veins with pyrite, bornite, etc. Two chalcopyrite types of are specific to the second productive substage. Chalcopyrite I forms xenomorphous segregations (up to 5 cm in size) and granular and disseminated aggregates, and chalcopyrite II occurs as thin disintegrated lamellae (up to 0.002 mm in size) in bornite. Sulfides in the ores amount to ≤3–5%. Calcite $Ca_{0.97}Fe_{0.02}Mn_{0.01}CO_{3.00}$ in the weathering crust is dissolved by surface waters or is replaced by malachite, smithsonite, etc. Native gold forms fine thin (0.002–1.2 mm) segregations in microcracks of rocks (skarns and aposkarn metasomatites) and in pyrite, chalcopyrite, and bornite. Gold is often intergrown with chalcopyrite, bornite, wittichenite, tetradymite, and pyrite (Figs. 4 and 5). In minerals of skarns, gold intergrown with chalcopyrite, bornite, and Bi–Te minerals is localized in cleavage cracks and pyroxene, amphibole, and chlorite interstices, thus reflecting the later deposition of productive mineral assemblage (Fig. 4*e*, *f*).

Gold forms fine thin (0.003–0.9 mm) lamellar, flattened, crack–veinlet, interstitial, pellet-like, lumpy, lumpy–branched, drop-like, and dendritic (flat, three-dimensional) segregations and intergrowths of crystals of combined rhombic-dodecahedron–cube and octahedral habits and is of mixed morphology (Fig. 6). The intergrowths of crystals of different habits resemble druses with differently oriented crystals (Fig. 6*g*). Euhedral gold grains with predominant octahedral and cube-octahedral habits are often found in chalcopyrite or limonite. There are often fine mosaic gold segregations with a block size of 0.5–7.0 μm, which intergrow with larger (up to 15 μm) euhedral gold crystals (Fig. 6*b*). The blocks in these segregations have clear borders. Gold varies in color from golden-yellow to bright yellow.

Native gold produced at the gold–telluride–sulfide–quartz–carbonate substage is of three types according to the content of gold:

(1) high-fineness gold with Ag ≤ 10 wt.% (Au = 89.58–92.04; Ag = 7.91–9.66; Cu = 0.00–0.26; and Hg = 0.00–0.05 wt.%);

(2) medium-fineness gold with Ag ≤ 19 wt.% (Au = 79.03–89.93; Ag = 9.91–19.05; Cu = 0.00–0.69; and Hg = 0.00–0.75 wt.%);

(3) low-fineness gold with Ag ≤ 24 wt.% (Au = 75.00–79.33; Ag = 20.24–24.14; Cu = 0.00–0.15; and Hg = 0.00–0.10 wt.%).

Table 2. Chemical composition of wittichenite, matildite, and tetradymite group minerals (wt.%)

Analysis	Bi	Te	Cu	S	Se	Sb	Total	Formula
	Second productive substage							
1	41.87	–	38.23	19.55	–	–	99.65	$Cu_{2.98}Bi_{1.00}S_{3.02}$
2	40.91	–	39.09	19.71	–	–	99.71	$Cu_{3.02}Bi_{0.96}S_{3.02}$
3	41.14	–	38.54	19.52	–	–	99.20	$(Cu_{3.01}Bi_{0.97}S_{3.02}$
4	40.67	–	39.02	19.52	–	–	99.21	$Cu_{3.03}Bi_{0.96}S_{3.01}$
5	41.89	–	38.40	19.51	–	–	99.80	$Cu_{2.99}Bi_{0.99}S_{3.02}$
6	57.17	–36.14	–	3.14	–3.02	–	99.47	$Bi_{1.97}Te_{2.04}(S_{0.71}Se_{0.28})_{0.99}$
7	56.59	35.49	–	2.62	4.41	–	99.11	$Bi_{1.97}Te_{2.03}(S_{0.59}Se_{0.41})_{1.00}$
8	58.67	36.5	–	3.54	1.25	–	99.96	$Bi_{2.03}Te_{2.06}(S_{0.80}Se_{0.11})_{0.91}$
9	58.10	35.59	–	3.21	3.05	–	99.95	$Bi_{2.00}Te_{2.00}(S_{0.72}Se_{0.28})_{1.00}$
10	58.44	35.48	–	3.56	2.12	–	99.60	$Bi_{2.01}Te_{2,00}(S_{0.80}Se_{0.19})_{0.99}$
11	58.60	35.48	–	3.77	1.73	–	99.58	$Bi_{2.01}Te_{1.99}(S_{0.84}Se_{0.16})_{1.00}$
12	56.72	38.49	–	2.62	1.86	–	99.69	$Bi_{2.00}(Te_{2.22}S_{0.60}Se_{0.18})_{3.00}$
13	51.47	47.56	–	–	–	–	99.03	$Bi_{1.99}Te_{3.01}$
14	51.89	47.56	–	–	–	–	99.45	$Bi_{2.00}Te_{3.00}$
15	52.14	47.25	–	–	–	–	99.39	$Bi_{2.01}Te_{2.99}$
16	52.38	46.90	–	–	–	0.32	99.60	$(Bi_{2.02}Sb_{0.02})_{2.04}Te_{2.96}$
17	52.05	46.89	–	–	–	0.36	99.30	$(Bi_{2.01}Sb_{0,.02})_{2.03}Te_{2.97}$
18	52.12	47.58	–	–	–	–	99.70	$Bi_{2.00}Te_{3.00}$
19	52.42	47.56	–	–	–	–	99.98	$Bi_{2.01}Te_{2.99}$
	Third productive substage							
20	62.51	37.39	–	–	–	–	99.90	$Bi_{1.01}Te_{0.99}$
21	63.06	36.74	–	–	–	–	99.80	$Bi_{1.02}Te_{0.98}$
22	62.47	37.13	–	–	–	–	99.60	$Bi_{1.01}Te_{0.99}$
23	63.14	36.64	–	–	–	–	99.78	$Bi_{1.03}Te_{0.97}$
24	63.03	36.91	–	–	–	–	99.94	$Bi_{1.02}Te_{0.98}$
25	62.11	37.84	–	–	–	–	99.95	$Bi_{1.00}Te_{1.00}$
26	54.74	28.92	–	16.41	–	–	100.7	$Ag_{1.03}Bi_{1.01}S_{1.96}$
27	68.51	31.42	–	–	–	–	99.93	$Bi_{4.00}Te_{3.00}$

Note. Analyses were carried out with a MIRA 3 LMU scanning electron microscope (analyst N.S. Karmanov, IGM SB RAS, Novosibirsk). 1–5, wittichenite; 6–12, Se-tetradymite; 13–19, tellurobismuthite; 20–25, tsumoite; 26, matildite; 27, pilsenite. Dash, below the detection limit.

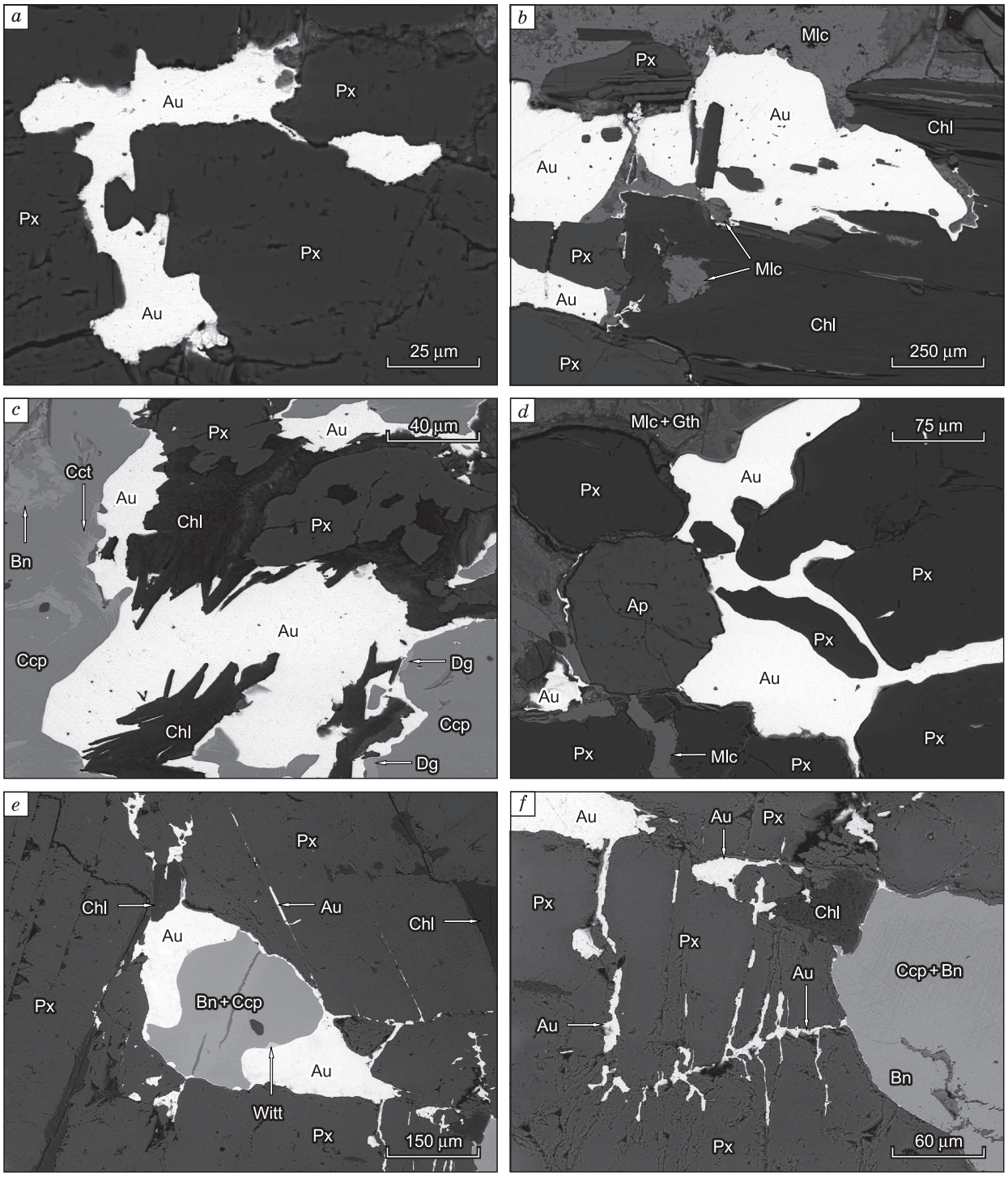

Fig. 4. Gold (Au), bornite (Bn), and halcopyrite (Ccp) of the second productive gold–telluride–sulfide–quartz–carbonate substage in microcracks of pyroxene skarns. Px, pyroxene; Chl, chlorite; Ap, apatite; Cct, chalcocite; Dg, digenite.

Wittichenite (Cu_3BiS_3) grains of different shapes (10–60 μm in size) were found in intergrowths with gold at the contact of bornite with disintegrated lamellae of chalcopyrite II (Figs. 4*e* and 5*a*, *b*).

Tetradymite ($Bi_2Te_2S_3$) occurs as fine inclusions (1–40 μm) in assemblage with wittichenite in bornite. It contains an impurity of Se (1.25–4.45 wt.%) and often has high contents of Te (Table 2).

Tellurobismuthite (Bi_2Te_3) is present as monomineral inclusions (5–100 μm in size) in chalcopyrite and bornite and in assemblage with tetradymite, hessite, and volynskite, sometimes forming rims over the latter (Fig. 5*e–g*). Some

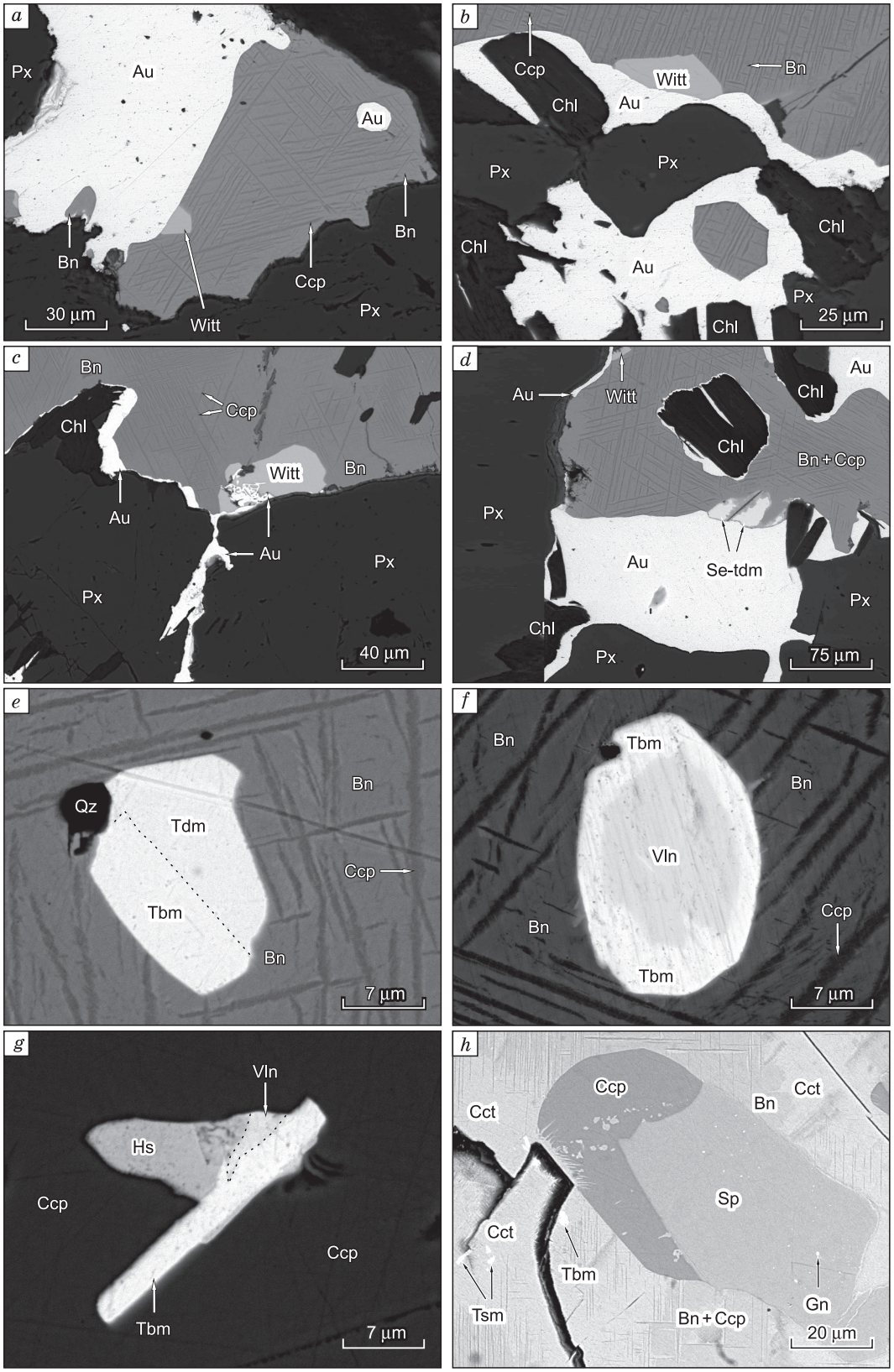

Fig. 5. Gold (Au), bornite (Bn), chalcopyrite (Ccp), wittichenite (Witt), tetradymite (Tdm), Se-tetradymite (Se-tdm), volynskite (Vln), tellurobismuthite (Tbm), hessite (Hs), sphalerite (Sp), galena (Gn), and tsumoite (Tsm) of the second productive gold–telluride–sulfide–quartz–carbonate substage in pyroxene skarns. Px, pyroxene; Chl, chlorite; Cct, chalcocite.

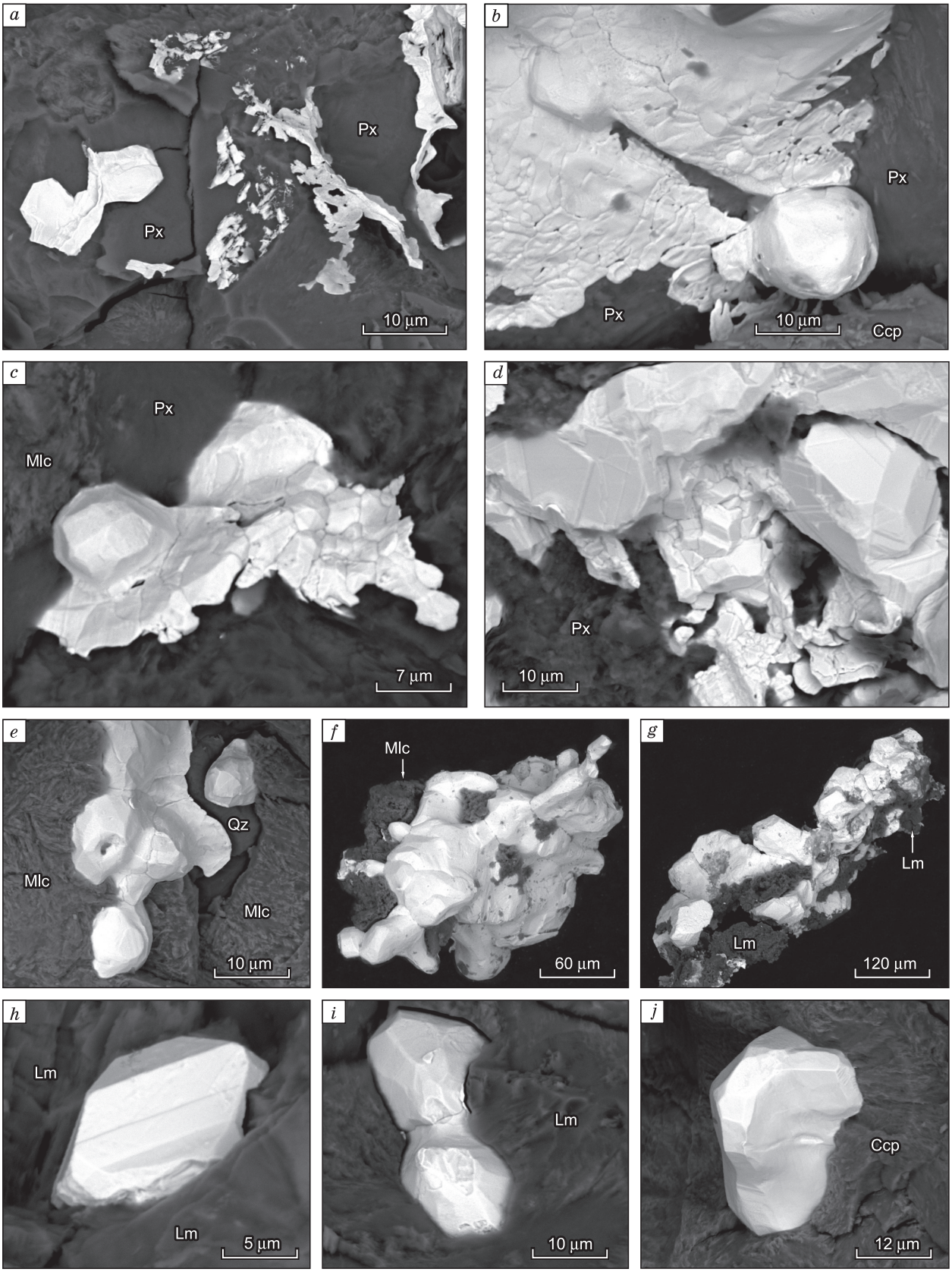

Fig. 6. Gold (Au) of the gold–telluride–sulfide–quartz–carbonate substage. Px, pyroxene, Ccp, chalcopyrite; Mlc, malachite; Qz, quartz; Lm, limonite.

Table 3. Chemical composition of volynskite, hessite, and acanthite (wt.%)

Run	Ag	Bi	Te	S	Total	Formula
Second productive substage						
1	18.89	36.28	44.29	–	99.46	$Ag_{1.01}Bi_{1.00}Te_{1.99}$
2	19.42	35.32	44.80	–	99.54	$Ag_{1.03}Bi_{0.97}Te_{2.00}$
3	61.75	–	38.25	–	99.99	$Ag_{1.97}Te_{1.03}$
4	62.40	–	37.57	–	99.97	$Ag_{1.99}Te_{1.01}$
Third productive substage						
5	62.67	–	37.05	–	99.42	$Ag_{2.00}Te_{1.00}$
6	62.36	–	36.87	–	99.23	$Ag_{2.00}Te_{1.00}$
7	62.76	–	36.81	–	99.57	$Ag_{2.01}Te_{0.99}$
8	61.98	–	37.32	–	99.30	$Ag_{1.98}Te_{1.01}$
9	86.92	–	–	–12.91	99.83	$Ag_{2.00}S_{1.00}$
10	87.54	–	–	12.30	99.84	$Ag_{2.04}S_{0.96}$

Note. Analyses were carried out with a MIRA 3 LMU scanning electron microscope (analyst N.S. Karmanov, IGM SB RAS, Novosibirsk). 1, 2, volynskite; 3–8, hessite; 9–10, acanthite. Dash, below the detection limit.

inclusions contain an impurity of Sb (up to 0.36 wt.%) (Table 2, analyses 16–17).

Hessite (Ag_2Te) of the second productive substage (5 to 15 μm) was found in intergrowths with tellurobismuthite, volynskite, and bornite in chalcopyrite.

Volynskite ($AgBiTe_2$) is intergrown with tellurobismuthite and hessite. The chemical compositions of Te and Bi minerals are stoichiometric or slightly deviate from the stoichiometric ones (Tables 2 and 3).

Mineralization of the late gold–sulfosalt–sulfide–quartz substage of the Tardan deposit is of limited occurrence and is found as thin (0.02–5 cm) veinlets in skarns and amphibole–chlorite and sericite–quartz metasomatites. Ore minerals amount to ≤1–2% and are chalcopyrite, pyrite, and sphalerite, which are densely intergrown with pilsenite, hessite, tsumoite, etc. (Fig. 7). The minerals of this substage cut and cement the mineral aggregates of the gold–telluride–sulfide–quartz–carbonate substage.

Gold of the late productive substage forms fine (0.005–1.000 mm) unevenly distributed interstitial, lumpy, lumpy-branched, and lumpy-cellular segregations, rounded or slightly faceted grains, and, more seldom, crystals of hexagonal, pentagon-dodecahedral, and combined cube-octahedral habits (Fig. 8). Some gold crystals have growth layers (Fig. 8*l*, *m*). Gold varies in color from golden-yellow to light yellow (silver-yellow). Some gold grains have a distinct zoning: The content of Au regularly decreases by 5–10 wt.% from core to rim, whereas the content of Ag increases (Au = 89.85 and Ag = 9.52 wt.% in the core; Au = 76.07 and Ag = 23.08 wt.% in the rim). Sometimes, the content of Au decreases from core (65.02 wt.%) to rim (45.13 wt.%) on the background of an increase in the contents of Ag (from 33.77 to 50.69 wt.%) and Hg (from 0.06 to 4.12 wt.%).

Native gold of the third productive substage is of four types according to the contents of Ag and Hg:

(1) medium-fineness gold with Ag ≤ 20 wt.% (Au = 80.49–89.09; Ag = 9.96–19.93; Cu = 0.00–0.78; and Hg = 0.00–0.87 wt.%);

(2) low-fineness gold with Ag ≤ 28 wt.% (Au = 71.53–80.13; Ag = 19.30–28.21; Cu = 0.00–0.80; and Hg = 0.00–0.13 wt.%);

(3) electrum with Ag ≤ 38 wt.% (Au = 60.96–69.01; Ag = 30.92–37.74; Cu = 0.00–0.03; and Hg = 0.00–0.81 wt.%);

(4) mercurian electrum with Ag ≤ 50 wt.% (Au = 45.13–47.44; Ag = 49.14–50.69; Hg = 3.03–4.12; and Cu = 0.00–0.01 wt.%).

Hessite (Ag_2Te) (grains 3–25 μm in size) of the gold–sulfosalt–sulfide–quartz substage is present in quartz, chalcopyrite, and pilsenite, is intergrown with gold, tsumoite, and Se-galena ($Pb_{0.97–1.01}Ag_{0.00–0.01}S_{0.89–0.90}Se_{0.10–0.13}$), and occurs in assemblage with bismuthinite, acanthite, matildite, baryte, etc.

Acanthite (Ag_2S) (grains up to 30 μm in size) is present in quartz, chalcopyrite, and pyrite. The composition of acanthite and hessite is presented in Table 3.

Tsumoite (BiTe) (grains up to 50 μm in size) is intergrown with chalcopyrite, hessite, and pilsenite in quartz.

Pilsenite (Bi_4Te_3) (grains up to 70 μm in size) and matildite ($AgBiS_2$) (grains measuring up to 20 μm) are in assemblage with the – mentioned above minerals in quartz and chalcopyrite (Fig. 7).

Native bismuth occurs as rounded phenocrysts in quartz.

Thus, we have established that the ores of the Tardan deposit contain native gold predominantly of high and medium fineness; ultrahigh- and low-fineness gold is subordinate, and electrum and mercurian electrum are scarce. The histogram of gold fineness shows three clear peaks corresponding to the recognized productive mineral assemblages (Fig. 9). The total average fineness of gold of the Tardan deposit varies from 451 to 986‰, averaging 858‰ (284 analyses). The fineness of gold of the first productive substage varies from 918 to 986‰, averaging 964‰; the fineness of gold of the second productive substage is 756–918‰, averaging 856‰; and the fineness of gold of the third productive substage is 452–897‰, averaging 756‰. All gold grains have a direct zoning: The contents of Ag and, sometimes, Hg increase

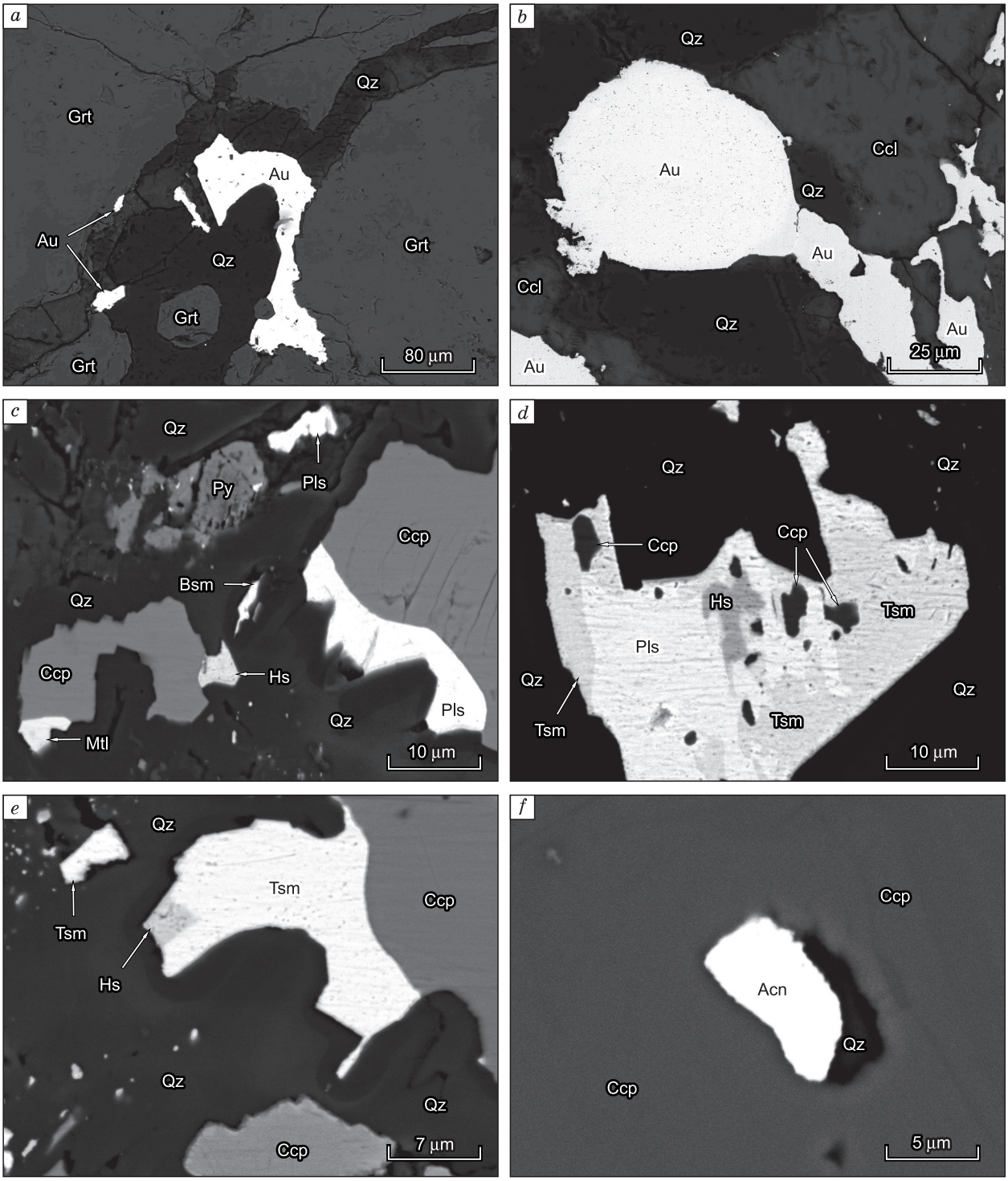

Fig. 7. Gold (Au), chalcopyrite (Ccp), pyrite (Py), pilsenite (Pls), hessite (Hs), bismuthinite (Bsm), matildite (Mtl), tsumoite (Tsm), acanthite (Can), and quartz (Qz) of the late gold–sulfide–quartz substage in assemblage with garnet (Grt) and chrysocolla (Ccl).

from core to rim. The zoning becomes more contrasting in passing from early to late gold generations.

Native gold forms the following trends: (1) gold of the gold–quartz–calcite substage: ultrahigh-fineness gold (Ag ≤ 4.80 wt.% and Hg ≤0.13 wt.%) → high-fineness gold (Ag ≤ 7.87 wt.% and Hg ≤ 0.04 wt.%); (2) gold of the gold–telluride–sulfide–quartz–carbonate substage: high-fineness gold (Ag ≤ 9.66 wt.% and Hg ≤ 0.15 wt.%) → medium-fineness gold (Ag ≤ 19.05 wt.% and Hg ≤ 0.75 wt.%) → low-fineness gold (Ag ≤ 24.14 wt.% and Hg ≤ 0.10 wt.%) ± hessite

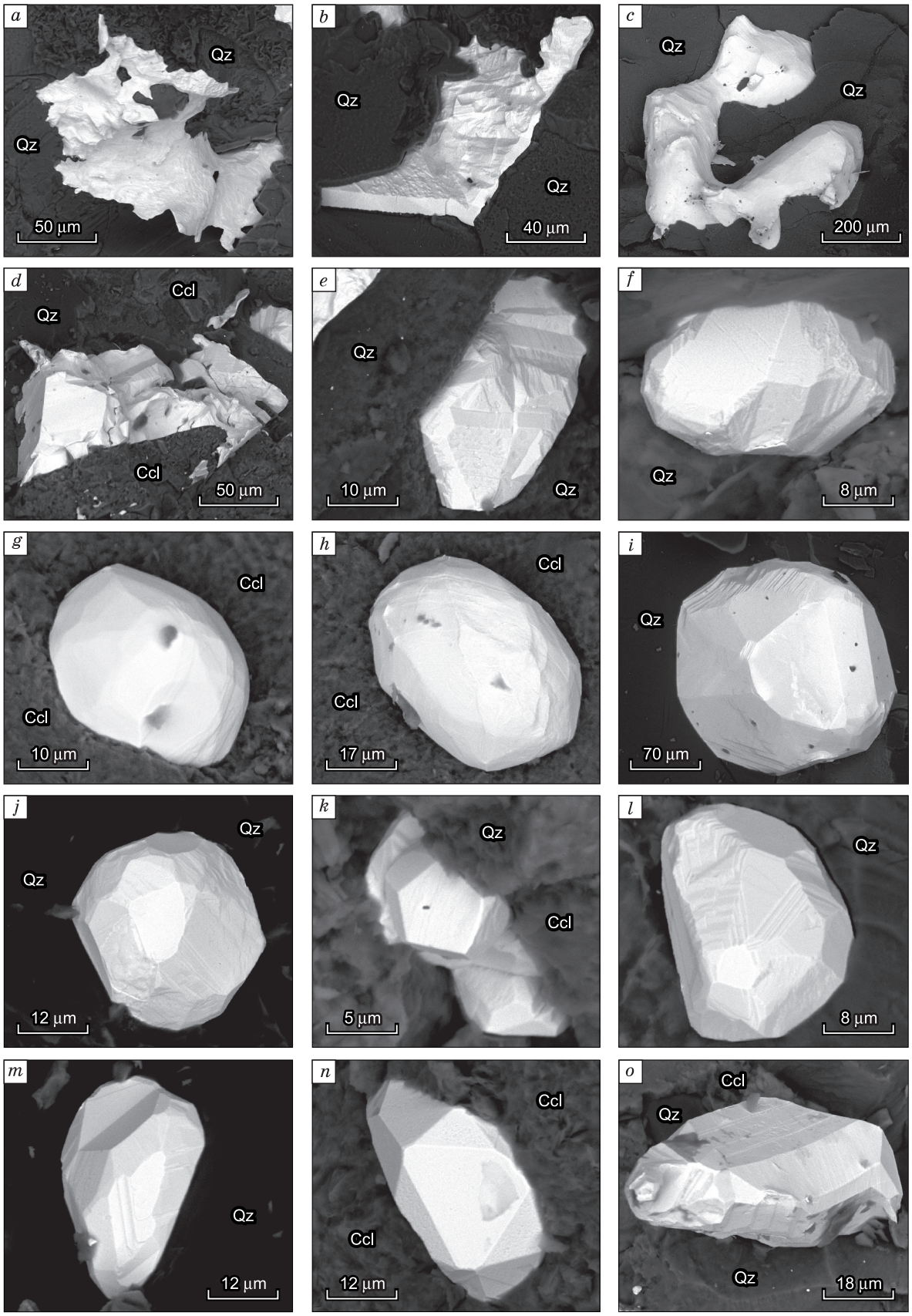

Fig. 8. Gold in quartz (Qz) and chrysocolla (Ccl) of the gold-sulfosalt-sulfide-quartz assemblage.

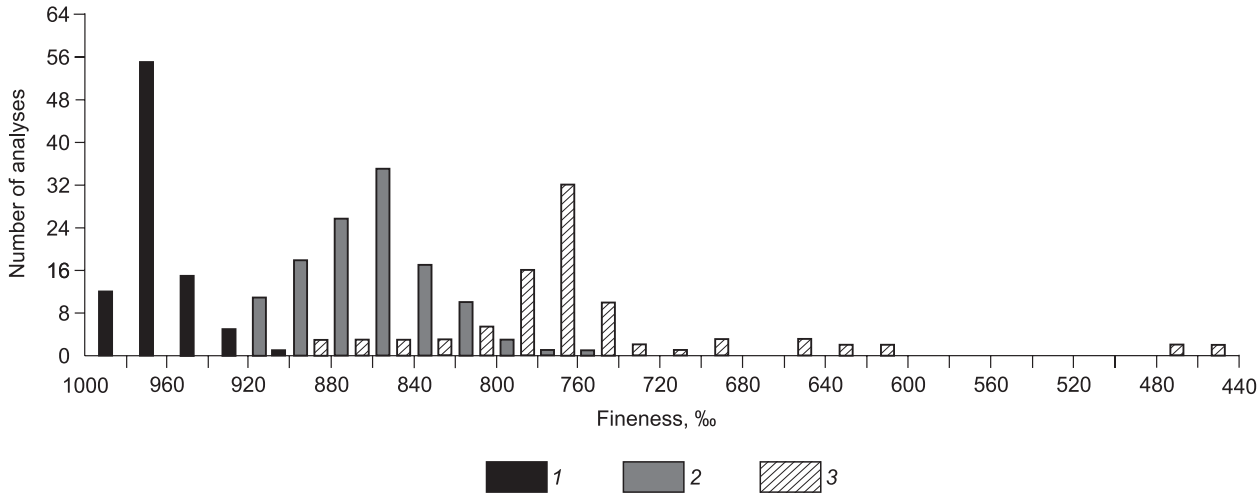

Fig. 9. Occurrence of the finenesses of native gold of the first (1), second (2), and third (3) productive substages in the Tardan deposit.

Ag_2Te ± volynskite $AgBiTe_2$; (3) gold of the gold–sulfosalt–sulfide–quartz substage: medium-fineness gold (Ag ≤ 19.93 wt.% and Hg ≤ 0.87 wt.%) → low-fineness gold (Ag ≤28.21 wt.% and Hg ≤ 0.13 wt.%) ± electrum (Ag ≤ 37.74 wt.% and Hg ≤ 0.81 wt.%) → mercurian electrum (Ag ≤ 50.69 wt.% and Hg ≤ 4.12 wt.%) ± hessite Ag_2Te ± acanthite Ag_2S ± matildite $AgBiS_2$.

THE CONDITIONS OF ORE MINERAL ASSEMBLAGES FORMATION

Gas'kov (2008) established that gold mineralization of the Tardan deposit formed over a wide temperature range (400–150 °C). The starting temperature of the first productive gold–quartz–calcite substage, determined from the pyrite–pyrrhotite solvus, is 380 ºC, with sulfur fugacity (f_{S_2}) of $10^{-7.6}$ (Toulmin and Barton, 1964). According to Gusev (2014), fluid inclusions (FI) in quartz of the early gold–quartz–calcite substage associated with pyrite, pyrrhotite, and arsenopyrite homogenized at 285–320 ºC.

A thermometric study was carried out for two-phase (vapor–liquid, VL) FI in isometric quartz grains (1–2 mm in size) from veinlets (up to 1.5 cm thick) formed at the gold–quartz–calcite substage. The inclusions are about 10–15 μm in size, isometric, rounded, with clear borders of vacuoles and with elements of crystal faces. They form groups (2–3 inclusions) or are localized singly in the cores of quartz grains or along the growth zones and are not observed in cracks. According to the classification by Roedder (1984), these are primary FI. The inclusions contain fluids with eutectic temperatures from –33.5 to –31.7 ºC, which indicates the presence of salts $MgCl_2$, NaCl, and KCl. The melting points of the last ice crystal in the FI are from –6.8 to –5.4 ºC, and the corresponding fluid salinity varies from 8.5 to 10.2 wt.% NaCl-equiv. The inclusions homogenized into a liquid at 270 to 300 ºC.

Quartz of the second productive gold–telluride–sulfide–quartz–carbonate substage is gray translucent, highly sheared and is found as individual grains and fragments 1–2 mm in size. At room temperature, syn-ore two-phase (VL) FI were identified, and they are isometric, 8–14 μm in size, isolated from each other, and irregularly distributed. The composition of their gas phase was not established because of the extremely low gas density. The homogenization temperatures were estimated at 275–360 ºC. The eutectic temperatures vary from –32 to –30 ºC, which indicates the presence of Na and Mg chlorides in the fluids. The concentrations of salts evaluated from the melting points of FI ice (–9 to –7 ºC) are 8.0–12.9 wt.% NaCl-equiv.

Primary FI in quartz and calcite of the third productive gold–sulfosalt–sulfide–quartz substage were also analyzed. Quartz forms as fine isometric transparent or translucent grains and thin veinlets in fine-grained calcite. Fluid inclusions in calcite were analyzed in large transparent grains. Two-phase (VL) FI are 10–15 or, less often, up to 20 μm in size; they form isolated groups (2–3 inclusions) in the grain cores and are not observed in the mineral cracks. Inclusions in quartz and calcite have similar geochemical and *P–T* parameters and contain fluids with eutectic temperatures from –37.8 to –31.0 ºC, which indicates the presence of Na, K, and Mg chlorides. The melting points of the last ice crystal vary from –6.0 to –3.8 ºC, and the fluid salinity varies from 6.1 to 9.2 wt.% NaCl-equiv. The inclusions homogenized into a liquid at 220–255 ºC.

Gas'kov (2008) established that at the final substage of mineral formation, a decrease in the temperature of hydrothermal fluids led to the deposition of chalcedony-like quartz associated with low-fineness gold and mercurian electrum. The homogenization temperature of FI in the chalcedony-like quartz is 150–200 ºC.

DISCUSSION

Hydrothermal gold mineralization of the Tardan deposit is of veinlet-disseminated and stockwork types and is also present in single quartz and sulfide–quartz veins. It is genetically related to medium-temperature pre-ore metasomatites of the listwanite–beresite series developed after skarns and intrusive rocks. The medium-temperature metasomatism is expressed mostly as listwanitization of skarns in tectonic crushing zones.

Native gold of the Tardan deposit was formed in three mineral substages. Productive mineral assemblages in serpentinites and metasomatites formed from Riphean–early Cambrian basic rocks include cobaltite, siegenite, and glaucodot atypical of hydrothermal gold deposits, which is due to the composition of the host rocks.

The deposition of productive mineral assemblages of the Tardan deposit involved medium-temperature (380–270 ºC and 360–275 ºC) and lower-temperature (255–150 ºC) medium-saline (6.1 to 12.9 wt.% NaCl-equiv) $MgCl_2$–NaCl–KCl–H_2O fluids. The mineralogical and *P–T* and geochemical data indicate that minerals of the first productive substage formed from fluids with salinity of 8.5–10.2 wt.% NaCl-equiv at 380–270 ºC. Paragenesis of pyrite, pyrrhotite, chalcopyrite, and arsenopyrite with native gold suggests f_{S_2} = $10^{-14.3}$–$10^{-7.6}$ at 300 ºC (Barton and Skinner, 1979; Afifi et al., 1988a,b).

Minerals of the second productive substage formed from fluids with salinity of 8.0 to 12.9 wt.% NaCl-equiv at 360–275 ºC. Paragenesis of tellurides and sulfides with bismuth sulfotellurides was controlled by the parameters of the medium near the stability field of pyrrhotite with f_{Te_2} = 10^{-11}–$10^{-10.2}$ and f_{S_2} = $10^{-11.3}$–$10^{-6.7}$ at 300 ºC. Thus, f_{Te_2} was below the stability limit of calaverite but within the stability field of tellurobismuthite and hessite. The overgrowth of volynskite with tellurobismuthite suggests an increase in f_{S_2}.

Mineral assemblages of the third productive substage were deposited from fluids with salinity from 6.1 to 9.2 wt.% NaCl-equiv at 255–150 ºC. At the final stage of mineral formation, the ore-bearing fluids were enriched in Ag and Hg, as evidenced by the evolution of native gold from medium-fineness gold to mercurian electrum and by the wide spread of Ag minerals (Ag_2Te, Ag_2S, and $AgBiS_2$). The high Ag/Au ratio in the ore-bearing fluids is confirmed by the presence of Ag_2S, because the earlier experiments showed (Pal'yanova et al., 2012) that Ag_2S precipitates at Ag:Au > 10. Ore deposition of the late productive stage proceeded with variations in f_{S_2}, as indicated by the replacement of early pyrrhotite by marcasite and pyrite; at the final stage, minerals were deposited at extremely low f_{S_2}. This explains the absence of cinnabar and the presence of metallic Hg in the form of mercurian electrum as well as pyrrhotite, native bismuth, and maldonite. Paragenesis of pyrrhotite, native bismuth, matildite, acanthite, and other sulfides indicates a change in the redox potential of ore-bearing fluids of the third productive substage with f_{S_2} = $10^{-17.8}$–$10^{-10.7}$ and f_{Te_2} = 10^{-17}–$10^{-11.4}$ at 200 °C (Barton and Skinner, 1979; Afifi et al., 1988).

Thus, the productive mineral assemblages of the Tardan deposit occured with a temperature decrease from early to late substages. The high salinity (up to 13 wt.% NaCl-equiv) and the presence of Mg chlorides in the fluid indirectly indicate the participation of magmatic fluids in the ore formation process (Wilkinson, 2001). The presence of Hg minerals also points to the involvement of magmatic fluids in the mineral formation, which confirms mercury outgassing in the mantle (Ozerova, 1986; Stepanov and Moiseenko, 1993). The wide destribution of Bi minerals in ores suggests a relationship between mineralization and granitoids, and the input of bismuth is apparently related to the granitoids of the Early Tannu-Ola complex (O_1tn), because Bi is a granitogene element (Savva, 2006; Goryachev and Gamyanin, 2010).

In the mineralogical and geochemical features the mineral assemblages of the first and second productive substages of the Tardan deposit are similar to the parageneses of the productive substages of the Barsuchii deposit of the Tardan ore cluster. In the Barsuchii deposit, minerals of the first gold–pyrrhotite–chalcopyrite–pyrite–quartz substage (quartz, pyrite, chalcopyrite, pyrrhotite, arsenopyrite, gold (Ag = 2.76–6.40 wt.% and Cu = 0.00–0.09 wt.%), calcite ± marcasite) and the second gold–telluride–pyrrhotite–chalcopyrite–pyrite–quartz substage (quartz, siderite, pyrite, chalcopyrite, pyrrhotite, arsenopyrite, solid solutions of minerals of the tellurobismuthite–tellurantimony series, gold (Ag = 6.73–21.92 wt.%), sphalerite, calaverite, ± petzite ± hessite ± galena ± Co-bearing arsenopyrite (Co ≤ 4 wt.%) ± cobaltite) are also localized in metasomatites of the listwanite–beresite series and in skarns and quartz diorites complicated by faults and secondary alterations. According to *P–T* and geochemical data, the minerals of the first productive substage of the Barsuchii deposit formed from CO_2- and methane-bearing Na–K chloride fluids with salinity of 1.7–10.5 wt.% NaCl-equiv at 360–280 ºC; and the minerals of the second productive substage formed from Mg, Na, and K chloride fluids with salinity of 5.0–8.8 wt.% NaCl-equiv at 330–240 ºC. During the mineral formation, the temperature of the ore-bearing fluid decreased from early to late substages. The $\delta^{34}S$ value of pyrite of the Barsuchii deposit lies in the narrow range from +1.4 to +4.6 ‰ and the sulfur isotope composition of fluid ($\delta^{34}S_{H_2S}$) in equilibrium with sulfides at the moment of mineral formation, calculated from equations of fractionation (Li and Liu, 2006), varies from +0.1 to +3.2 ‰, which indicates the participation of magmatic source of sulfur (0 ± 5 ‰) [Ohmoto, 1986]..

The mineral assemblages of the third productive substage of the Tardan deposit are similar to the parageneses of the gold–sulfosalt–sulfide–quartz substage (quartz, chalcopyrite, pyrite, baryte, galena (Ag ≤ 1.18 wt.%), By-bearing Zn-tennantite–tetrahedrite, matildite $AgBiS_2$, aikinite $CuPbBiS_3$, berryite $Cu_3Ag_2Pb_3Bi_7S_{16}$, pyrrhotite, bismuthinite,

native bismuth, gold (Ag = 15.51–29.41 wt.%), electrum (Ag = 31.13–62.20 wt.%), mercurian electrum (Ag = 32.11–65.74 wt.% and Hg = 1.10–8.45 wt.%), kustelite, and Hg-kustelite (Ag = 68.16–72.42 wt.% and Hg = 0.00–7.47 wt.%) of the Tardan-2 ore occurrence in the beresitized plagiogranites of the Early Tannu-Ola complex (O_1tn) (Kuzhuget et al., 2018). Gold of the Tardan-2 ore occurrence is also characterized by a distinct zoning of grains, expressed as a decrease in Au content by 5–50 wt.% from core to rim and an increase in Ag and Hg contents. The contents of Hg and Ag show a direct correlation. Some gold grains change in composition from core to rim (wt.%): (1) medium-fineness gold (Au = 80.45 and Ag = 20.09) → mercurian electrum (Ag = 65.74, Au = 32.80, and Hg = 2.17) → mercurian kustelite (Au = 71.86, Ag = 27.47, and Hg = 1.29) and (2) electrum (Ag = 68.12 and Au = 26.99) → mercurian kustelite (Ag = 72.42, Au = 20.99, and Hg = 7.47). The mineral assemblages of the productive substage of the Tardan-2 ore occurrence crystallized from NaCl–KCl–H_2O and $MgCl_2$–H_2O fluids with salinity of 1.7–8.7 wt.% NaCl-equiv in hypabyssal conditions (P ~ 0.73–0.98 kbar; ~2.1–3.0 km) at 280–120 ºC.

The mineralogical and geochemical features of the ores of the Tardan and Barsuchii deposits and the Tardan-2 ore occurrence show that these objects are derivates of a single ore-magmatic system. In the Tardan ore cluster, hydrothermal gold mineralization in stockworks with scarce veins is of three productive assemblages, which are of different abundance in the studied objects. In the Tardan deposit, ~25% Au is present in the early productive assemblage; ~70% Au, in the second; and ~5% Au, in the third. In the Barsuchii deposit, there are only the first and the second productive assemblages, and in the Tardan-2 ore occurrence, only the third assemblage is present. Correspondingly, the Tardan and Barsuchii deposits bear early medium-temperature mineral assemblages with gold, and the Tardan-2 ore occurrence, late low-temperature mineral assemblage with baryte, native bismuth, and gold with wide variations in fineness (Ag ≤ 72.42 wt.% and Hg ≤ 8.45 wt.%). The following sequence of formation of gold parageneses is observed in the Tardan ore cluster: early (quartz, calcite, pyrite, pyrrhotite, arsenopyrite, ultrahigh-fineness and high-fineness gold ± chalcopyrite ± sphalerite ± marcasite) → intermediate (quartz, calcite, chalcopyrite, galena ± bornite, pyrite, wittichenite, volynskite, tellurobismuthite, tetradymite, sphalerite, high-, medium-, and low-fineness gold ± cobaltite) → late (quartz, calcite, chalcopyrite, pyrite, baryte, galena, Zn-tennantite–tetrahedrite, matildite, acanthite, medium- and low-fineness gold, electrum, mercurian electrum ± kustelite ± mercurian kustelite ± aikinite ± berryite ± bismuthinite ± Bi-tellurantimony ± native bismuth).

In mineralogical and geochemical compositions the objects of the Tardan ore cluster are similar to gold–bismuth deposits (Gamyanin et al., 1998, 2003; Goryachev and Gamyanin, 2006), which are intrusion-related deposits according to the classification by Lang and Baker (2001), i.e., pluton-related hydrothermal gold deposits (Spiridonov, 2010).

Typical gold–bismuth deposits are the Pogranichnoe (East Sayan), Ergelyakh, Kurumskoe, Tuguchak, Basagun'-inskoe, Chuguluk, Nenneli, and Galechnoe (northeastern Russia) vein and Levodybinskoe and Teutedzhak (northeastern Russia) stockwork deposits confined to the apical contact zones of granitoid plutons or to their marginal contact zones complicated by faults (Gamyanin et al., 1998; Goryachev et al., 2004; Damdinov et al., 2009; Garmaev et al., 2013; Vikent'eva et al., 2018). The most famous world gold deposits of this geochemical type (Fort Knox, Pogo, Golden Horn, and Nixon Fork in Alaska) are intrusion-related (Gamyanin et al., 2017).

The above gold–bismuth deposits of Russia are characterized by a low-sulfide (≤3%) ore composition and a wide variety of Bi minerals (native bismuth, Bi tellurides and sulfotellurides, bismuthinite, ikunolite, maldonite, etc.). The early productive mineral assemblages of these deposits are arsenide–sulfarsenide complexes including Co and Ni minerals with a wide Fe–Co–Ni isomorphism. The late productive parageneses comprise gold–bismuth minerals of the bismuth–sulfotelluride–quartz type (Goryachev and Gamyanin, 2006; Gamyanin et al., 2017). Gold–bismuth deposits form at rhe expense of to aqueous fluids with Na and K chlorides (46.0–1.1 wt.%) over a wide range of temperatures (437–155 ºC; mostly, 400–250 ºC) and pressures (1700–90 bars) and under variations in f_{O_2}–f_{S_2} (Gamyanin et al., 2017; Vikent'eva et al., 2018).

CONCLUSIONS

Thus, native gold of the Tardan hydrothermal deposit was deposited throughout three mineral formation substages. According to the composition of productive mineral assemblages, the deposit is of gold–sulfide type, with Bi–Ag telluride and sulfotellurides features. The assemblages of late substages include Bi–Te minerals.

Mineralogical and geochemical studies have revealed native gold mostly of high and medium fineness in the Tardan ores. Ultrahigh- and low-fineness gold is subordinate, and electrum and mercurian electrum are scarce. The fineness of the Tardan gold varies from 451 to 986‰, averaging 858‰.

The mineral assemblages of the deposit crystallized from $MgCl_2$–NaCl–KCl–H_2O fluids with salinity of 6.1–12.9 wt.% NaCl eq., on the background of a temperature decrease from 380 to 150 ºC and variations in f_{O_2}, f_{S_2}, f_{Se_2}, and f_{Te_2}, which were reflected in the chemical composition of gold and ore mineral composition (the presence of pyrrhotite, native bismuth, maldonite, mercurian electrum, etc.).

The high salinity (up to 13 wt.%), the presence of Mg salts in the ore-forming fluids, and the presence of Hg minerals indirectly suggest the involvement of magmatic fluids in the mineral formation.

The hydrothermal gold mineralization of the Tardan deposit is genetically related to pre-ore medium-temperature metasomatites of the listwanite–beresite series. This suggests that the deposit is of stockwork type with pluton-related hydrothermal low-sulfide gold–quartz mineralization. By geochemical typification, it is similar to orogenic intrusion-related Au–Bi deposits.

We thank E.K. Druzhkova for help in petrographic research. The mineralogical and geochemical studies were financially supported by grant 17-45-170970 p_a from the Russian Foundation for Basic Research The study of fluid inclusions was carried out on state assignments of IGM SB RAS (project 0330-2016-0002) and IM SU FRS MG UB RAS (2019–2021). The field studies were performed on state assignments of TuvIENR SB RAS (project 0384-2016-0012).

REFERENCES

Afifi, A.M., Kelly, W.C., Essene, E.J., 1988a. Phase relations among tellurides, sulfides, and oxides: I. Thermochemical data and calculated equilibria. Econ. Geol. 83, 377–394.

Afifi, A.M., Kelly, W.C., Essene, E.J., 1988b. Phase relations among tellurides, sulfides, and oxides: II. Applications to telluride-bearing ore deposits. Econ. Geol. 83, 395–404.

Barton, P.B., Skinner, B.J., 1979. Sulfide mineral stabilities, in: Barnes, H.L. (Ed.), Geochemistry of Hydrothermal Ore Deposits. John Willey & Sons, New York, pp. 278–403.

Berzin, N.A., Kungurtsev, L.V., 1996. Geodynamic interpretation of Altai–Sayan geological complexes. Geologiya i Geofizika (Russian Geology and Geophysics) 37 (1), 63–81 (56–73).

Berzin, N.A., Coleman, R.G., Dobretsov, N.L., Zonenshain, L.P., Xiao Xuchang, Chang, E.Z., 1994. Geodynamic map of the western part of Paleoasian Ocean. Geologiya i Geofizika (Russian Geology and Geophysics) 35 (7–8), 8–28 (5–22).

Bodnar, R.J., Vityk, M.O., 1994. Interpretation of microthermometric data for H_2O–NaCl fluid inclusions, in: Fluid Inclusions in Minerals: Methods and Applications. Virginia Polytechnic Institute and State University, Pontignana-Siena, pp. 117–130.

Borisenko, A.S., 1977. Study of the salt composition of solutions of gas–liquid inclusions in minerals by the cryometric method. Geologiya i Geofizika (Russian Geology and Geophysics) 18 (8), 16–28 (11–19).

Borisenko, A.S., 1982. Cryometric analysis of the salt composition of fluids of gas–liquid inclusions in minerals, in: Laverov, N.P. (Ed.), Using Methods of Fluid Inclusion Study in Search for and Exploration of Ore Deposits [in Russian]. Nedra, Moscow, pp. 37–46.

Damdinov, B.B., Garmaev, B.L., Mironov, A.G., Dashinmaev, Z.B., 2009. Gold-bismuth mineralization in the southeastern part of the Eastern Sayan. Dokl. Earth Sci. 425 (2), 256–259.

Distanov, E.G., Obolenskii, A.A., 1994. Metallogenic development of the Central Asian mobile belt in relation to its geodynamic evolution. Geologiya i Geofizika (Russian Geology and Geophysics) 35, (7–8), 252–269 (218–234).

Gamyanin, G.N., Goncharov, V.I., Goryachev, N.A., 1998. Gold–rare-metal deposits of northeastern Russia. Tikhookeanskaya Geologiya 17 (3), 94–103.

Gamyanin, G.N., Goryachev, N.A., Bakharev, A.G., Kolesnichenko, P.P., Zaitsev, A.I., Diman, E.N., Berdnikov, N.V., 2003. Genesis and Evolution Conditions of Magmatic Granitoid Gold Ore Systems in the Mesozoids of Northeastern Asia [in Russian]. SVKNII DVO RAN, Magadan.

Gamyanin, G.N., Vikent'eva, O.V., Prokof'ev, V.Yu., 2017. Isotope-geochemical composition of ore-forming fluids in gold–bismuth deposits of northeastern Russia, in: Geology and Mineral Resources of Northeastern Russia. Proceedings of the Seventh All-Russian Science and Practice Conference Dedicated to the 60th Anniversary of the Institute of Diamond and Precious Metal Geology, SB RAS (Yakutsk, 5–7 April 2017) [in Russian]. Izdat. Dom SVFU, Yakutsk, Vol. 1, pp. 46–51.

Garmaev, B.L., Damdinov, B.B., Mironov, A.G., 2013. Pogranichnoe Au–Bi occurrence, Eastern Sayan: composition and link to magmatism. Geol. Ore Deposits 55 (6), 455–466.

Gas'kov, I.V., 2008. New data on the correlation of skarn and gold mineralization at the Tardan deposit (northeastern Tuva). Russian Geology and Geophysics (Geologiya i Geofizika) 49 (12), 923–931 (1227–1237).

Goryachev, N.A., Gamyanin, G.N., 2006. Gold–bismuth (gold–rare-metal) deposits of northeastern Russia: types and commercial exploration prospects, in: Gold Deposits of Eastern Russia [in Russian]. SVNTs DVO RAN, Magadan, pp. 50–62.

Goryachev, N.A., Gamyanin, G.N., 2010. Bismuth in orogenic gold deposits of northeastern Asia, in: Native Gold: Typomorphism of Mineral Assemblages, Formation Conditions of Deposits, and Applied Research Problems. Proceedings of the All-Russian Conference (with International Participants) in Memory of N.V. Petrovskaya (1910–1991) [in Russian]. IGEM RAN, Moscow, Vol. 1, pp. 159–161.

Goryachev, N.A., Newberry, R.J., Gamyanin, G.N., Layer, P.W., McCoy, D.T., Church, S.E., 2004. Granitoid-related gold lode deposits over the Northern pacific marginal areas, in: Metallogeny of the Pacific Northwest. Tectonics, Magmatism and Metallogeny of Active Continental Margins. Proceedings of the Interim IAGOD Conference (1–20 September, 2004). Dalnauka, Vladivostok, pp. 199–201.

Gusev, A.I., 2014. Gold mineralization of the Tardan ore cluster in eastern Tuva. Sovremennye Naukoemkie Tekhnologii, No. 3, 77–81.

Kil'chichakov, K.M., Tokunov, V.F., Plekhanov, A.I., 1966. Results of the Assessment of the Tardan Gold Deposit Potential and Gold Prospecting in the Bai-Syut River Basin [in Russian]. Izd. TGRE, Kyzyl.

Korobeinikov, A.F., Matsyushevskii, A.V., 1976. Gold in intrusive and contact-metasomatic rocks of the Tardan skarn field in Tuva. Geokhimiya, No. 9, 1409–1416.

Korobeinikov, A.F., Zotov, I.A., 2006. Regularities of the Formation of Gold Skarn Deposits [in Russian]. Izd. TPU, Tomsk.

Korobeinikov, A.F., Nomokonova, G.G., Erofeev, L.Ya., 1987. Regularities of the formation of gold mineralization in the geologic, geochemical, and physical fields of contact aureoles of granite intrusions. Geologiya Rudnykh Mestorozhdenii 29 (2), 58–70.

Korobeinikov, A.F., Anan'ev, Yu.S., Gusev, A.I., Voroshilov, V.G., 2013. Ore-Metasomatic and Geochemical Zoning of Gold Ore Fields and Deposits in the Fold Belts of Siberia [in Russian]. Izd. Tomskogo Politekhnicheskogo Universiteta, Tomsk.

Kudryavtseva, A.I., 1969. Some regularities of gold distribution in skarn minerals of the Tardan deposit, in: Materials on the Geology of the Tuva ASSR [in Russian]. Tuvinskoe Knizhnoe Izd., Kyzyl, Issue 1, pp. 68–72.

Kuzhuget, R.V., Prokop'ev, I.R., Redina, A.A., Oorzhak, Sh.N., 2018. Mineralogical and geochemical specifics and PTX conditions of formation of the Tardan-2 gold–sulfide–quartz ore occurrence (northeastern Tuva), in: Geology, Magmatism, and Metallogeny of the Center of Asia, 2018: Ore-Magmatic Systems of Sangilen (Alkaline Intrusions and Carbonatites). Proceedings of the First All-Russian Field Conference with International Participants [in Russian]. TuvIKOPR SO RAN, Kyzyl, pp. 72–76.

Lang, J.R., Baker, T., 2001. Intrusion related gold systems: the present level of understanding. Miner. Deposita 36, 477–489.

Li Y., Liu J., 2006. Calculation of sulfur isotope fractionation in sulfides. Geochimica Cosmochimica Acta. 70, 1789–1795.

Mongush, A.A., 2016. Basalt complexes of the Sayan–Tuva fore-arc zone: geologic location, geochemistry, and geodynamics, in: Natural Resources of Tuva and Adjacent Regions of Central Asia: State and Exploration. Ecological and Economic Problems of Nature Management [in Russian]. TuvIKOPR SO RAN, Kyzyl, Issue 14, pp. 74–94.

Ohmoto, H., 1986. Stable isotope geochemistry of ore deposits. Rev. Mineral. 16, 491–560.

Ozerova, N.A., 1986. Mercury and Endogenous Ore Formation [in Russian]. Nauka, Moscow.

Pal'yanova, G.A., Kokh, K.A., Seryotkin, Yu.V., 2012. Formation of gold–silver sulfides and native gold in Fe–Ag–Au–S system. Russian Geology and Geophysics (Geologiya i Geofizika) 53 (4), 347–355 (450–460).

Petrovskaya, N.V., 1973. Native Gold [in Russian]. Nauka, Moscow.

Rafailovich, M.S., 2013. Gold skarn deposits of Central Asia: geologic location, chemical composition, and ore potential. Izvestiya Natsional'noi Akademii Nauk Respubliki Kazakhstan. Seriya Geologii i Tekhnicheskikh Nauk, No. 1, 1–28.

Rafailovich, M.S., Shevchuk, S.I., 2010. Gold-bearing skarns of Central Asia. Geologiya i Okhrana Nedr, No. 1, 23–34.

Roedder, E., 1984. Fluid Inclusions. Rev. Mineral. Mineralogical Society of America, Vol. 12.

Rudnev, S.N., Vladimirov, A.G., Ponomarchuk, V.A., Bibikova, E.V., Sergeev, S.A., Matukov, D.I., Plotkina, Yu.V., Bayanova, T.B., 2006. The Kaa-Khem polychronous granitoid batholith (eastern Tuva): composition, age, sources, and geodynamic setting. Litosfera, No. 2, 30–42.

Rudnev, S.N., Serov, P.A., Kiseleva, V.Yu., 2015. Vendian–Early Paleozoic granitoid magmatism in Eastern Tuva. Russian Geology and Geophysics (Geologiya i Geofizika) 56 (9), 1232–1255 (1572–1600).

Savva, N.E., 2006. Gold–rare-metal ore association of northeastern Russia: sources of material, in: Ore Genesis and Metallogeny of East Asia. Proceedings of the Conference Dedicated to the 100th Birthday of B.L. Flerov [in Russian]. YaGU, Yakutsk, pp. 157–159.

Sovluk, A.V., 2010. Tectonic structure of the Tardan gold deposit (Republic of Tyva) as a basis for the prediction for commercial gold mineralization on its flanks. Nauka i Sovremennost', No. 1, 80–83.

Spiridonov, E.M., 2010. Review of gold mineralogy in major types of Au mineralization, in: Gold of the Kola Peninsula and Adjacent Regions. Proceedings of the All-Russian (with International Participants) Scientific Conference Dedicated to the 80th Anniversary of the Kola Science Center, Russian Academy of Science (Apatity, 26–29 September 2010) [in Russian]. Izd. K&M, Apatity, pp. 143–171.

Stepanov, V.A., Moiseenko, V.G., 1993. Geology of Gold, Silver, and Mercury. Part 1. Gold–Mercury Deposits [in Russian]. Dal'nauka, Vladivostok.

Toulmin, P., Barton, P.B., 1964. A thermodynamic study of pyrite and pyrrhotite. Geochim. Cosmochim. Acta 28 (5), 641–671.

Vakhrushev, V.A., 1972. Mineralogy, Geochemistry, and Formation of Skarn Gold Deposits [in Russian]. Nauka, Novosibirsk.

Vernadsky, V.I., 1914. The Experience of Descriptive Mineralogy [in Russian]. Izd. Imperatorskoi Akademii Nauk, Petrograd.

Vikent'eva, O.V., Prokofiev, V.Yu., Gamyanin, G.N., Goryachev, N.A., Bortnikov, N.S., 2018. Intrusion-related gold–bismuth deposits of North-East Russia: *PTX* parameters and sources of hydrothermal fluids. Ore Geol. Rev. 100, 240–259.

Wilkinson, J.J., 2001. Fluid inclusions in hydrothermal ore deposits. Lithos 55, 229–272.

Yarmolyuk, V.V., Kovalenko, V.I., Kovach, V.P., Kozakov, I.K., Kotov, A.B., Sal'nikova, E.B., 2003. Geodynamics of Caledonides in the Central Asian Foldbelt. Dokl. Earth Sci. 389A (3), 311–316.

Zonenshain, L.P., Kuz'min, M.I., Natapov, L.M., 1990. Plate Tectonics of the USSR Territory [in Russian]. Nedra, Moscow, Book 1.

Editorial responsibility: A.S. Borisenko